RSC Advances

ROYAL SOCIETY OF CHEMISTRY

www.rsc.org/advances

Effect of particle size on the surface activity of TiC-Ni composite coating via the interfacial valence electron localization

Zirun Yang [a, b] • Hao Lu [b] • Ziran Liu [b] • Xianguo Yan [c] • Dongyang Li [b, c*]

Abstract Electron work functions (EWF) and open potentials of electrodeposited nickel, TiC microparticle-reinforced and TiC nanoparticle-reinforced Ni matrix coatings were studied with the objective to investigate effects of TiC particle size on the surface activity and corrosion tendency of the coatings. First-principles calculation was conducted to elucidate the underlying mechanism. Results of the study demonstrate that the overall EWF and open potential of Ni coating decreased when TiC microparticles (diameter = 2μm) were added. However, TiC nanoparticles (diameter = 200 nm) showed opposite effects. Such changes are ascribed to the effect of particle size on the TiC/Ni interfacial state. It was shown that TiC microparticle/Ni interface had a low interfacial EWF. While the TiC nanoparticle resulted in a stronger TiC/Ni interface with elevated EWF. The first-principles calculation revealed that valence electrons were more localized in the region of nano TiC/Ni interface, resulting in higher EWF, stronger interfacial bonding, and higher surface stability that limited electrons to participate in corrosion reactions.

Keywords Particles size · Surface activity · Corrosion · Electron work function · Electron localization

* Correspond author: Email: dongyang.li@ualberta.ca (Dongyang Li)

[a] School of Materials Engineering, Yancheng Institute of Technology, No.211 Jianjun East Road, Yancheng, 224051, P.R China

[b] Department of Chemical and Material Engineering, University of Alberta, Edmonton, Alberta, Canada T6G2G6

[c] School of Mechanical Engineering, Taiyuan University of Science and Technology, Taiyuan, Shanxi, 030024, P.R China

Introduction

Particle-reinforced metal-matrix composites (PRMMCs) generally exhibit desired mechanical properties. However, when used in corrosive environments, PRMMCs may suffer from galvanic corrosion. Pardo et al. [1] showed increased corrosion rate and spalling of the corrosion product scale of SiC particle reinforced AZ92 Mg alloy (particle size: 5μm) in a 3.5wt% NaCl solution. However, the corrosion behavior of composites is still not fully understood. Karunanithi et al [2] demonstrated that adding TiO_2 particles to Al 7075 alloy raised its corrosion potential with lowered corrosion current in a 3.5wt% NaCl solution but the corrosion current increased when more than TiO_2 (>10vol%) was added. Thorough elucidation of the mechanisms responsible for the phenomena need more studies. It appears that corrosion of PRMMCs is largely affected by the particle size, which affects the particle/matrix interface. For ceramic reinforced PRMMCs, the general nonconductive behavior of ceramics prevents them to act as micro-cathodes. In this case, the ceramic/matrix interfacial regions, which are generally defected and strained, may act as anodes and degrade faster than the matrix, leading to faster material deterioration [1–5]. Hence, the interface between the particle and matrix plays a crucial role especially when the reinforcing particles are nonconductive. The interfacial properties are affected by the interfacial mismatch stress and defects. A smaller particle may have lower interfacial stress and fewer defects. It was observed that TiC nanoparticle-Ni composite coatings exhibited lower corrosion currents and higher corrosion potentials [6]. The fraction of nanoparticles also affects the corrosion resistance. Venkatesha et al [7] showed that the polarization potential of ZrO_2 nanoparticle-Zn was elevated with increasing the volume fraction of the ZrO_2 nanoparticles.

Corrosion involves charge transfer, affected by the electron activity and passivation if materials are passive [8]. Thus, it is of importance to look at the electron behavior of various phases and interfaces in order to understand why the nanoparticle reinforced MMCs perform differently from microparticle

reinforced ones. In recent years, the electron work function (EWF) has received increasing attention for studying corrosion phenomena [9, 10]. EWF refers to the minimum energy needed to move electrons at Fermi level inside a metal to its surface without kinetic energy [11]. This parameter is not only a measure of the surface activity but also related to many intrinsic material properties [9]. EWF is readily measured by the scanning Kelvin force microscopy (SKPFM). Local EWF can be analyzed and mapped using a nano-Kelvin probe attached to a multimode atomic force microscope (AFM), which can also map other properties and topography simultaneously. Such maps are particularly useful in identifying desired and undesired phases and interfaces.

The study reported in this article was inspired by recent research [12] on EWF and corrosion of SiC nanoparticle-reinforced Al composites, which showed increased corrosion resistance with the incorporated SiC nanoparticles. Such improvement appears to be ascribed to the electron localization at SiC/Al interface, leading to elevated overall work function. Such a phenomenon is not expected for conventional composites. For larger particles, the interfacial mismatch stress increases, which generally weaken the interface with lowered EWF. With the motivation of understanding how the particle size affects EWF across the ceramic/metal interface and how this influences the overall work function and corresponding corrosion potential, the authors conducted the present study.

Electrodeposited TiC-Ni coating was selected as a sample material for this study. Electroplating is one of coating processes, e.g., making hard Cr and alloy coatings [13], for protecting materials from wear and corrosion. However, the toxicity issues involved in Cr plating [14] and complicated alloy deposition processes [15,16] affect application of electrodeposited coatings. The development of co-electrodeposition technique for making composite coatings [17,18] much facilitates developing coatings with higher protection capability. However, composites may suffer from galvanic corrosion and are thus more susceptible to corrosive environments. Use of nano-sized reinforcements has shown

great promise of eliminating or minimizing such a drawback. Understanding the size effect of particles on the corrosion tendency of PRMMCs is the driving force for this study. Selecting Ni as the matrix material is attributed to facts that Ni is easy to be electrodeposited and Ni has good compatibility with many materials, which is used as a bond coat [19]. Ni is also a common matrix material for composite coatings [20, 21]. With sufficient knowledge of nickel, selection of Ni as a matrix material in this study makes relevant analyses easier. Using TiC as the reinforcing phase is attributed to its high hardness and well established database of its properties.

The objective of this study is to investigate effects of ceramic particle size on the electron behavior and surface activity of PRMMCs. Particular attention was put on interfacial electron activity and its influences on the corrosion tendency (open potential), evaluated using a multi-mode atomic force microscope and an electrochemical system. First-principles calculation was implemented to investigate the interfacial mismatch strain, corresponding electron localization and the electron work function, a measure of electron activity for participating corrosion reactions. Although this study is conducted for a specific material, the obtained knowledge is general, which would not only help look in fundamental issues but also benefit material design for optimized performance of composite coatings.

Experimental and calculation details

Materials and Fabrication

304 stainless steel plates (wt%: C 0.08%, Mn 2.0%, Si 1.05, P 0.04%, S 0.03%, Cr 3.64%, Ni 9.0%, balanced by Fe) were used as cathodes on which TiC/Ni coatings were electrodeposited. A plate of Nickel (99.98% purity, from Sigma Aldrich) was used as the anode. TiC microparticles (particle diameter d = 2 μm, provided by Sigma Aldrich) and nanoparticles (d=200 nm, provided by Sigma Aldrich) were used as the reinforcing phase, respectively. Prior to electrodeposition, the 304 stainless

steel plates were polished with emery paper up to grade 2400, rinsed with distilled water.

The electrolyte for electrodeposition of pure Ni, TiC microparticle- and nanoparticle- reinforced Ni coatings was a Watt′s-type bath, which contained $NiSO_4 \cdot 6H_2O$ (250 g l^{-1}), $NiCl_2 \cdot 6H_2O$ (45 g l^{-1}), H_3BO_3 (40 g l^{-1}), Hexadecylpyridinium bromide (100 g l^{-1}) and sodiumlauryl sulphate (200 g l^{-1}). These chemical reagents were purchased from Sigma Aldrich. All chemicals were used as received without any further treatment. pH value of the electrolyte was adjusted by adding sulfuric acid or dilute sodium hydroxide solutions. TiC particles were added to the electrolyte, which was magnetically stirred at 300 rpm min-1 during deposition in order to maintain a uniform distribution of TiC particles in the electrolyte. All coatings plated at current density 2 A dm^{-2} and voltage 2 V at 50~60 $^{\circ}$C. The plating time was 30 min and the electrodeposited rate was 7 μm min^{-1}. The thickness of electrodeposited TiC-Ni coatings was about 200 μm.

Characterization and Evaluation

Open circuit potentials (OCP) of the coatings in a 3.5wt% NaCl (NaCl+H_2O) solution were measured using a computerized Gamary Instruments Framework PC4/750 electrochemical system. A saturated calomel electrode (SCE) was used as the reference electrode and a platinum plate with an area of 1 cm^2 was used as the counter electrode. A scan rate of 0.1 mV s^{-1} was used to obtain open potential curves. Prior to the electrochemical tests, each specimen connected a copper wire was mounted in epoxy resin with a surface area of 1 cm^2 exposed to the corrosive solution. Before testing, the exposed surface was polished with silicon carbide papers up to 2400-grit and cleaned with acetone.

A scanning Kelvin probe (SKP) system (KP Technology Ltd., Caithness, UK) was used to measure EWFs of coatings with TiC particles of two different sizes. The KP system had three sub-systems (a digital oscillator, data acquisition, and sample translation) controlled by a host PC. A three-axis

microstepper positioner permitted high-resolution sample positioning (0.4 μm per step) and the scanning area was 2 mm ×2 mm. A gold tip with diameter equal to 1 mm was used. The EWF value was obtained by averaging EWF values collected from 100 points over the scanned area. The oscillation frequency of the Kelvin Probe was 173 Hz. Before testing, the exposed surface was ground with silicon carbide papers up to 2400-grit and cleaned with acetone.

An AFM equipped with a doped silicon tip coated by magnetic CoCr was used to measure the surface topography and contact potential difference. The topography of sample surface was obtained in the first scan in tapping mode. During the second scan, the cantilever was lifted up by 100 nm to rule out the influence of the surface topography on contact potential signals. In contact potential difference measurement, obtained values of Volta potentials are relative to the probe, which can be converted to EWF.

Computational analysis

Ni-TiC supercells were computationally analyzed using the density functional theory (DFT) as implemented in the Vienna Ab initio Simulation Package (VASP) [22,23] with projector-augmented wave (PAW) potential [24]. The generalized gradient approximation (GGA) with the exchange-correlation functional of Perdew (PW91) was employed [25]. Convergence tests indicated that 520 eV was a sufficient cutoff for PAW potential to achieve high precision in our system. K-points sampling using Monkhorst-Pack with k-mesh of 17×17×1 are sufficient for structure optimization [26]. We found that a denser k-mesh (25×25×1) was necessary for calculating the electron localization function for the supercells.

Results and discussion

Fig. 1 presents typical 3-dimension AFM topography images with different particle sizes. As

shown in Fig. 1a, the TiC microparticles are sparsely distributed in the Ni matrix. While the nanoparticles are densely and evenly distributed in the Ni matrix as shown in Fig. 1b. In order to view the nanoparticles, the scanned surface area covered by the nanoparticles had dimensions of $1\mu m \times 1\mu m$, while that covered by the microparticles were $20\mu m \times 20\mu m$. It should be pointed out that the TiC particles appear to be somewhat elongated but they are actually spherical. The topographic image may not reflect the exact surface morphology, which is influenced by the bond-order between the probe and the sample.

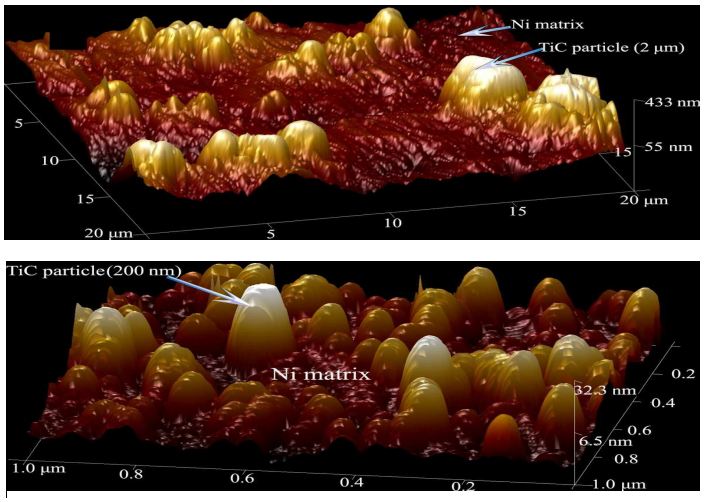

Fig.1 3-dimension AFM topography images: (a) TiC (2 μm)/Ni coating and (b) TiC (200 nm)/Ni coating. Scan rate: 1.00 Hz

Open potential tests were performed to evaluate the surface activity of the three coatings in a 3.5wt% NaCl solution. Fig. 2 illustrates measured open potentials of the coatings. As demonstrated, the TiC (2 μm)/Ni coating had lower open potential, compared to the pure Ni coating. While TiC (200 nm)/Ni coating showed higher open potential than the pure Ni coating. Clearly, the added TiC nanoparticles reduced the tendency of Ni to corrosion, while the TiC microparticle showed an opposite effect.

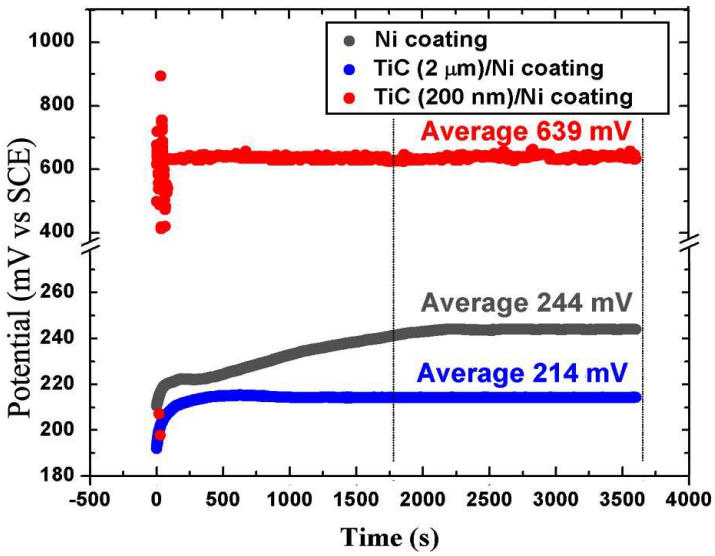

Fig. 2 Open potential curves of three coatings. Scan rate: 0.1 mV s^{-1}

Fig. 3 illustrates representative EWF of the coatings. Similar to the open potentials, EWF generally decreased as TiC microparticles were added. While the TiC nanoparticles markedly increased the overall EWF, corresponding to an increase in the surface inertness to electrochemical attack.

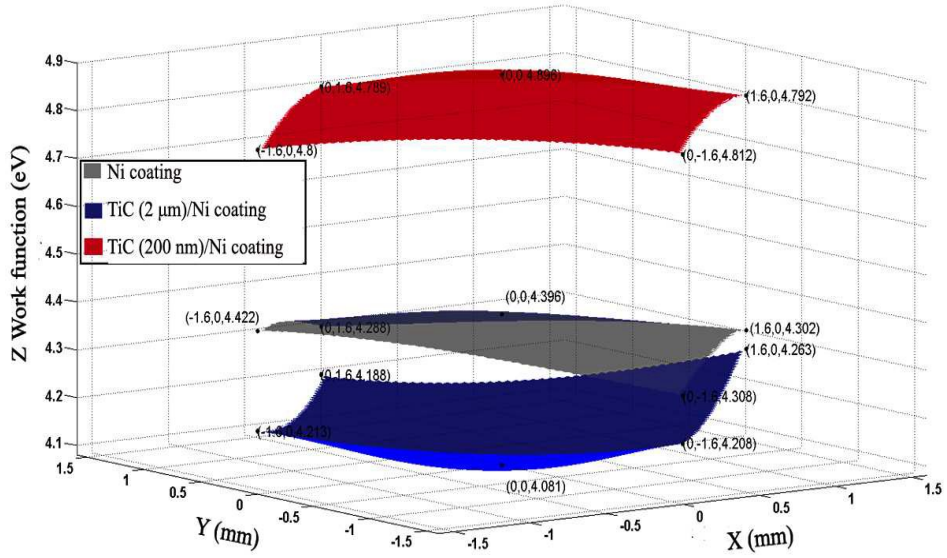

Fig. 3 EWF distributions of three coatings measured by SKP. Scan rate: 173 Hz

Corrosion is an electrochemical reaction during which a metal losses electrons and dissolves in a corrosive solution. The activity of electrons is reflected by the work function, which is the minimum

energy required to move electrons at Fermi level from inside a metal to its surface with zero kinetic energy [11,27]. A higher work function corresponds to a larger resistance to electrochemical reaction and is thus related to a higher open potential as Fig. 2 illustrates. In the present case, TiC microparticles decreased the open potential and work function of Ni coating, while TiC nanoparticles showed opposite effects, suggesting that the TiC nanoparticles reduced the electrochemical driving force. Since TiC is a ceramic with a higher work function and poor electrical conductivity, which remains insert in the solution, it should not act as a micro-cathode relative to Ni, causing local galvanic corrosion. Instead, the interfacial zone between the TiC and Ni matrix could be more anodic than the Ni matrix, resulting in local galvanic corrosion. In order to see whether this is the case, the contact potential difference in different surface locations of the coatings were measured using a multi-mode AFM with a silicon tip coated by magnetic CoCr. Fig.4(a) illustrates a surface potential map of the coating with TiC microparticles. The surface contact potential difference of the TiC (2 μm)/Ni coating distributes unevenly. The darker area represents lower contact potential difference, i.e. higher work function. A representative line potential profile is given in Fig.4(b). As shown, at the interface between a TiC particle and the Ni matrix, the potential decreases, corresponding to lowered work function. This implies that the Ni matrix may act as cathode and the interfacial zones act as anode, resulting local galvanic corrosion at the TiC/Ni interface. The added TiC microparticles, forming a large number of micro galvanic cells consisting of the TiC/Ni interfacial zones and Ni matrix, accelerated corrosion when the coating was exposed to the corrosive solution.

However, the nanoparticles showed relatively even potential or work function distribution as Fig. 5 illustrates. The work function of the composite coating was higher than that of Ni. This indicates that the TiC nanoparticles may constrain surrounding electronic activities and make electrons less easy to escape. As a result, the TiC nanoparticles added Ni coating has an enhanced inertness to corrosion and

local galvanic corrosion is suppressed by the added TiC nanoparticles.

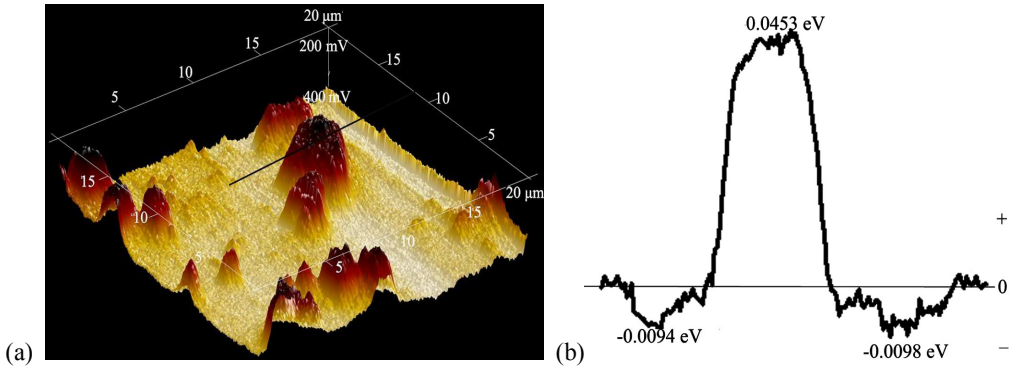

Fig. 4 (a) A contact potential map of TiC (2 μm)/Ni coating measured by AFM. Scan rate: 1.00 Hz; (b) Variations in the contact potential along a line across a TiC particle (marked in fig.4(a)).

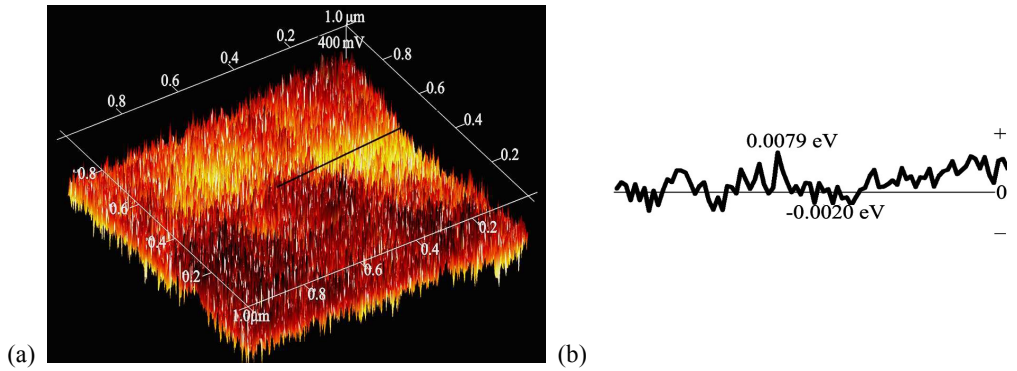

Fig.5 (a) A contact potential map of TiC (200 nm)/Ni coating measured by AFM. Scan rate: 1.00 Hz; (b) Variations in the contact potential along a line marked in fig.4(a).

The different effects of TiC particles with different sizes on work function and its distribution should be largely related the behavior of TiC/Ni interface, which is influenced by the particle size that can affect interfacial coherence and the interfacial stress caused by the lattice mismatch between TiC and Ni matrix. The interfacial stress certainly affects the interfacial electron behavior and thus work function. Especially for nanoparticles with a very large overall interfacial area, the interfacial influence becomes particularly important.

The rise in EWF is an indication of an increase in valence electron density [27], corresponding to a decrease in the polarizability [28]. The latter is a measure of the degree of easy for charge redistribution in an external field. A decrease in polarizability makes the material more resistant to external fields or

less active [29]. Thus, the TiC nanoparticles can raise the work function with lowered polarizability, resulting in reduced chemical reactivity.

For better understanding the effect of TiC particle size on the performance of the composite coatings, first-principles calculations were carried out to investigate the behavior of electrons in the TiC/Ni interfacial region. The electron localization functions (ELF) were calculated. ELF is defined as [30,31]

$$\mathrm{ELF} = \frac{1}{1+\left(\frac{D(\vec{r})}{D_h(\vec{r})}\right)^2} \tag{1}$$

where

$$D(\vec{r}) = \frac{1}{2}\nabla_{\vec{r}}\nabla_{\vec{r}'}\rho(\vec{r},\vec{r}')\Big|_{\vec{r}=\vec{r}'} - \frac{1}{8}\frac{\left|\nabla n(\vec{r})\right|^2}{n(\vec{r})} \tag{2}$$

and

$$D_h(\vec{r}) = \frac{3}{10}\left(3\pi^2\right)^{2/3} n(\vec{r})^{5/3} \tag{3}$$

ρ is the first-order reduced density matrix with spin dependence, $D(\vec{r})$ is the kinetic energy functional, $D_h(\vec{r})$ is the kinetic energy density of uniform electron gas with a spin density equal to the local $n(\vec{r})$. ELF is ranged from 0 to 1. High ELF values mean that that at given positions the electrons are more localized than in a uniform electron gas of the same density. ELF=0.5 indicates that the effect of the Pauli repulsion is the same as in the uniform electron gas of the same density.

The first-principle calculation was implemented to investigate how the mismatch strain affected electron localization at the interface and thus the interfacial behavior. Results of the calculation are presented in Fig.6. The main purpose of the calculation is to understand and explain the observed changes in EWF with respect to the particle size rather than providing precise quantitative information. The following three general cases were studied:

1) When the TiC particle was extremely small, its surface atoms had much low confinement from atoms inside the bulk, so that the surface atoms could match the matrix to form an interface with near-zero interfacial strain. In this case, atoms in a computed supercell could be relaxed, forming a strong interface between TiC and Ni matrix, which shows a higher ELF as illustrated in Fig. 6(a). A higher degree of electron localization renders electrons harder to escape, corresponding to a higher work function and consequently larger resistances to corrosion and mechanical attacks.

2) For larger particles, inclusions and thin films, the interfacial strain resulting from the lattice mismatch generally increases as the domain size or film thickness increases [20, 21, 32]. When the TiC particle size was large (Fig. 6(c)), Ni crystal around TiC particles was stretched and Ni atoms were separated in order to keep coherent at the interface with the TiC particle. If no dislocations formed at the interface, the mismatch strain would be quite high. For simplicity without losing the physical significance, we treated a case in which the mismatch strain was about 11% as Fig.6(c) illustrates. This interface had large interfacial mismatch strain energy, resulting in weaker bond between the TiC particle and the Ni matrix. Such an interface is not only mechanically weaker but also less resistant to electrochemical attacks due to its less stable electronic state.

3) In general, the interfacial mismatch strain rises as the TiC size increases. As a matter of factor, the lattices could be dislocated in order to minimize the interfacial strain energy. We used a supercell with 4 lattice sites of TiC to match 5 lattice sites of Ni while kept the lattice constant of Ni =3.524 Å (see Fig.6(b)). With this configuration, the interfacial mismatch strain energy

was considerably reduced through the formation of dislocations, compared to the case shown in Fig.6(c). The interface was incoherent and corresponding EWF and open corrosion potential were lowered but not as low as those caused by larger interfacial mismatch strain without the generation of interfacial defects.

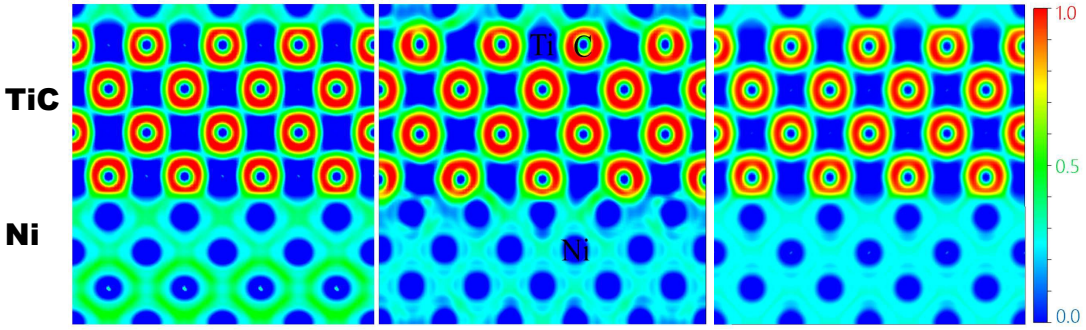

(a) (b) (c)

Fig. 6 Electron localization functions of TiC/Ni supercells determined by first-principles calculations. (a) For a small TiC particle, TiC is coherent with fcc Ni having a lattice constant of a=3.524 Å, the Griffith work of the interface is 0.553 eV/atom; (b) For a larger TiC particle, a supercell with 4 lattices of TiC and 5 lattices of Ni was built, the constant of Ni still was a=3.524 Å. In this case, the strain energy was partially released through formation of dislocations. The Griffith work of this incoherent interface is 0.448 eV/atom. (c) For larger TiC particle, if no dislocations form at the interface, the interfacial strain increases considerably. Let the lattice constant of Ni equal to a=3.926 Å, which is an average of 4.328 Å (TiC) and 3.524 Å, the Griffith work of the interface is 0.374 eV/atom.

The work function at interface is an indicator of its bond strength. Griffith work of the interfaces under study was calculated, which shows that the Griffith work of the coherent interface (Fig.6(a)) is 0.553 eV/atom, followed by that of the incoherent interface (Fig.6(b)) that is equal to 0.448 eV/atom, and the one without dislocations (Fig.6(c)) is 0.374 eV/atom. Such variations in the interfacial bonding results from the changes in electron localization that is related to the degree of ease for electron to migrate at the interface or the interfacial electron work function, which is influenced by the TiC particle size.

The changes in EWF in the vicinity of TiC/Ni interface resulted in corresponding changes in the overall EWF as Fig.3 illustrates. Such phenomena are explainable. Fig. 7 schematically illustrates how

the overall work function is influenced by the TiC particle size. For TiC microparticle-reinforced Ni coating, the lower interfacial EWF decreases the overall EWF, bear in mind that electrons escape from lower EWF regions when EWF is measured. For TiC nanoparticle-reinforced Ni coating, the enhanced interfacial electron localization raises the EWF near the coherent interface. In addition, the reduced spacing between TiC nanoparticles may cause EWF overlap as illustrated in Fig.7. As a result of the above two factors, a higher overall EWF could be generated.

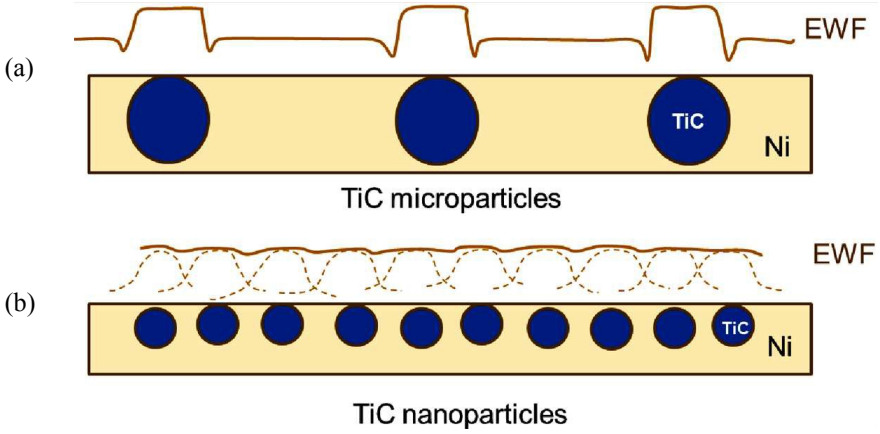

Fig. 7 (a) For a TiC microparticle-reinforced Ni coating, the lower EWF at TiC/Ni interface decreases the measured overall EWF, bear in mind that electrons escape from lower EWF regions when EWF is measured. (b) For TiC nanoparticle-reinforced Ni coating, the enhanced interfacial electron localization raises the EWF near the TiC/Ni interface. In addition, the reduced spacing between TiC nanoparticles may cause EWF overlap. As a result of the two factors, a higher overall EWF could be generated.

Up to this point, we attribute the decreased tendency of corrosion of TiC nanoparticle–reinforce Ni coating mainly to the enhanced electron localization. There are also other possible factors influencing the corrosion resistance of the composite coatings, such as the grain size, growth of corrosion products and effective metallic area, etc. However, these factors may not play a main role in affecting the corrosion potential and EWF. The following are reasons:

a) Influences of matrix's grain size and corrosion products

Due to the heterogeneous nucleation mechanism, the TiC nanoparticles may promote

nucleation of Ni, resulting smaller grains (on nano-scale). For passive metals, nano-sized grains improve the passive oxide film (due to enhanced atomic diffusion along grain boundaries, which may increase the oxide adherence and integrity), leading to raised EWF. Anwar Ul-Hamid et al [33] investigated corrosion behaviors of nanocrystalline and coarse-grained Ni samples in a 3.5 wt% NaCl solution, and showed that the nanocrystalline Ni had a higher corrosion potential, about 0.06V higher than that of the coarse-grained Ni. In the present case when tested also in a 3.5wt%NaCl solution, the increase in corrosion potential of Ni with TiC nanoparticle is about 0.43V (7 times as large as 0.06V). Thus, if the improvement in corrosion behavior of small-grained Ni is ascribed to the reduction of grain size and better oxide film, such roles should still be minor, compared to the role of electron localization as described in this article.

b) Effective metallic area

The effective metallic area can affect the corrosion kinetics or corrosion rate but not much the corrosion potential or tendency. Thus, the effective metallic area should not largely influence the corrosion potential and electron work function.

Conclusions

Electron work functions and open potentials of Ni, TiC microparticle-Ni and TiC nanoparticle-Ni electrodeposited coatings were investigated experimentally and computationally. The TiC microparticles decreased EWF and open potential of the composite coating, which should be largely attributed to lowed EWF at the TiC/Ni interface. While the TiC nanoparticles showed opposite effects. The first-principles calculation revealed that electrons were more localized in the region of nano TiC/Ni interface, resulting in higher EWF and consequently a stronger interfacial bonding as well as a

higher barrier to hinder electrons from participating in corrosion reactions. However, the electron localization function (ELF) at the interface between TiC microparticle and the Ni matrix is lower with formation of poor bond or no bond, which is more prone to corrosion. The lowered ELF is caused by larger interfacial mismatch strain.

Acknowledgment

This work is supported by the Natural Science and Engineering Research Council of Canada, Auto21, Jiangsu Government Scholarship for Overseas Studies and Natural Science Foundation of Jiangsu Province, China (Grant No. BK2012250), Suncor Energy, GIW, Shell Canada, Magna International, and Volant Products Inc.

References

1 A. Pardo, S. Merino, M.C. Merino, I. Barroso, M. Mohedano, R. Arrabal, F. Viejo, Corros Sci, 2009, **51**, 841-849.

2 R. Karunanithi, S. Bera, K.S. Ghosh, Mater Sci Eng, 2014, **B190**, 133-143.

3 S. Candan, E. Bilgic, Mater Lett, 2004, **58**, 2787-2790.

4 L.Q. Guo, M. Li, X.L. Shi, Y. Yan, X.Y. Li, L.J. Qiao, Corros Sci, 2011, **53**, 3733-3741.

5 F. Toptan, A.C. Alves, I. Kerti, E. Ariza and L.A. Rocha, Wear, 2013, **306**, 27–35.

6 M. Raja, G. N. K. Ramesh Bapu, J. Maharaja and R. Sekar, Surf. Eng, 2014, **30**, 697-701.

7 Kanagalasara Vathsala and Thimmappa Venkatarangaiah Venkatesha, Appl Surf Sci, 2011, **257**, 8929-8936.

8 William D. Callister, David G. Rethwisch, Materials science and engineering: an introduction. 2000, Wiley & Sons Inc, New York.

9 X.Y. Wang and D.Y. Li, Electrochimica Acta, 2002, **47**, 3939-3947.

10 M. Li, L.Q. Guo, L.J. Qiao and Y. Bai, Corros Sci, 2012, **60**, 76-81.

11 M.P. Marder, Condensed matter physics, 2000, John Wiley and Sons Inc, New York, USA.

12 Sareh Mosleh-Shirazi, Guomin Hua, Farshad Akhlaghi, Xianguo Yan, Dongyang Li, Scientific Report 2015, DOI: 10.1038/srep18154.

13 A. El Hajjami, M.P. Gigandet, M. De Petris-Wery, J.C. Catonne, J.J. Duprat, L. Thiery, F. Raulin, N. Pommier, B. Starck, P. Remy, Appl Surf Sci, 2007, **254**, 480-489.

14 H. Royle, Environmental Research, 1975, **10**, 141-163.

15 C.N.ANAGOPOULOS, P.E. AGATHOCLEOUS, V.D. PAPACHRISTOS, A. MICHAELIDES, Surface and Coatings Technology, 2000, **123**, 62-71.

16 H van Oosterhout, AMP Journal of Technology, 1992, **2**, 63-69.

17 F. C. Walsh and C. Ponce de Leon, Transactions of the IMF, 2014, **2**, 82-88.

18 Alain Robin, Júlio Cesar Pinheiro de Santana, Antonio Fernando Sartori, Surface and Coatings Technology 2011, **205**, 4596-4601.

19 Z. Yu, D.D. Hass, H.N.G. Wadley, Materials Science and Engineering A 2005, **394**, 43-52.

20 P. Baghery, M. Farzam, A. B. Mousavi and M. Hosseini, Surf. Coat. Tech. 2010, **204**, 3804-3810.

21 G. Parida, D. Chaira, M. Chopkar and A. Basu, Surf. Coat. Tech. 2011, **205**, 4871-4879.

22 G. Kresse, J. Non-Cryst. Solids 1995, **192&193**, 222-229.

23 G. Kresse, J. Furthmüller, Comp. Mater. Sci. 1996, **6**, 15-50.

24 G. Kresse, D. Joubert, Phys. Rev. B 1999, **59**, 1758.

25 John P. Perdew, J. A. Chevary, S. H. Vosko, Koblar A. Jackson, Mark R. Pederson, D. J. Singh and Carlos Fiolhais, Phys. Rev. B 1992, **46**, 6671.

26 Hendrik J. Monkhorst and James D. Pack, Phys. Rev. B, 1976, **13**, 5188–5192.

27 G.M. Hua and D.Y. Li, Appl. Surf Sci., 2011, **99**, 041907 1–3.

28 N.H. March and M.P. Tosi, J Mol Struc-THEOCHEM, 1995, **343**, 199–201.

29 D.S. Sabirov, RSC Adv, 2014, **4**, 44996–45028.

30 L.De Santis and R. Resta, Surface Science, 2000, **450**, 126-132.

31 A. Savin, R. Nesper, S. Wengert and T.F. Fassler, Angewandte Chemie-International Edition in English, 1997, **36**, 1809-1832.

32. James M. Howe, Interfaces in Materials, 1997, John Wiley & Sons, Inc., New York.

33. Anwar Ul-Hamid , Abdul Quddus, Huseyin Saricimen, Hatim Dafalla, Materials Research, 2015, **18**, 20-26.